The Astrophysical Journal, 788:84 (11pp), 2014 June 10 doi:10.1088/0004-637X/788/1/84

PHASE-RESOLVED *XMM-NEWTON* AND *SWIFT* OBSERVATIONS OF WR 25

J. C. Pandey, S. B. Pandey, and Subhajeet Karmakar
Aryabhatta Research Institute of Observational Sciences (ARIES), Nainital 263 002, India; jeewan@aries.res.in
Received 2013 September 25; accepted 2014 April 28; published 2014 May 23

ABSTRACT

We present an analysis of long-term X-ray and optical observations of the Wolf–Rayet binary, WR 25. Using archival data from observations with the *XMM-Newton* and the *Swift* observatories, spanning over ∼10 yr, we show that WR 25 is a periodic variable in X-rays with a period of 208 ± 3 days. X-ray light curves in the 0.5–10.0 keV energy band show phase-locked variability, where the flux increased by a factor of ∼2 from minimum to maximum, being maximum near periastron passage. The light curve in the soft energy band (0.5–2.0 keV) shows two minima indicating the presence of two eclipses. However, the light curve in the hard energy band (2.0–10.0 keV) shows only one minimum during the apastron passage. The X-ray spectra of WR 25 were explained by a two-temperature plasma model. Both the cool and the hot plasmas were constant at 0.628 ± 0.008 and 2.75 ± 0.06 keV throughout an orbital cycle, where the cooler plasma could be due to small scale shocks in a radiation-driven outflow and the high temperature plasma could be due to the collision of winds. The column density varied with the orbital phase and was found to be maximum after the periastron passage, when the WN star is in front of the O star. The abundances of WR 25 were found to be non-solar. Optical *V*-band data of WR 25 also show the phase-locked variability, being at maximum near periastron passage. The results based on the present analysis indicate that WR 25 is a colliding wind binary where the presence of soft X-rays is attributed to individual components; however, hard X-rays are due to the collision of winds.

Key words: binaries: general – stars: early-type – stars: individual (WR 25) – stars: winds, outflows – stars: Wolf–Rayet – X-rays: stars

Online-only material: color figures

1. INTRODUCTION

Massive O-type stars evolve into Wolf–Rayet (WR) phases when their hydrogen fuel has been consumed and products of nuclear fusion appear in their atmosphere, before ending their lives as core-collapse supernovae (Doom 1987; Smartt et al. 2009; Smartt 2009). Typically, the progenitors of WR stars have initial masses greater than 25 $M_{\odot}$ (Crowther 2007) and they spend ∼10% of their ∼5 Myr lifetime in the WR phase (Meynet & Maeder 2005). Spectra of WR stars are predominantly characterized by emission lines of He and N (WN stars), He and C (WC stars), and He and O (WO stars). In the evolutionary sequence of massive stars, WC and WO stars are expected to correspond to later stages than WN stars. WR stars are known to produce strong stellar winds driven by their strong radiation field. The stellar winds can reach velocities up to 1000–3000 km s^{-1} with mass-loss rates of 10^{-4} to 10^{-6} $M_{\odot}$ yr^{-1}, depending upon mass and age (Hamann et al. 2006). These winds not only affect the evolution of WR stars but also have a tremendous impact on their ambient media. The detailed physical properties of WR stars are summarized in many past reviews (e.g., Abbott & Conti 1987; van der Hucht 1992; Crowther 2007).

X-ray emissions from WR binaries may consist of the combined emission from intrinsic stellar wind shocks and colliding wind shocks between the two binary components (Prilutskii & Usov 1976; Cherepashchuk 1976; Luo et al. 1990; Usov 1992; Stevens et al. 1992). Colliding wind binary systems often exhibit periodic X-ray modulation either because of the change in binary separation or due to the changing circumstellar opacity along the line of sight to the collision zone, resulting from the orientation of the system with respect to the observer. Serious investigations of these variations were carried out after the advent of high-quality facilities like *XMM-Newton* and *Chandra*. Many O+O and WR+O binaries, as observed with *XMM-Newton*, show different kinds of phase-locked modulations, e.g., V444 Cyg and CD Cru (Bhatt et al. 2010b), HD 159176 (De Becker et al. 2004), HD 152248 (Sana et al. 2004), HD 93403 (Rauw et al. 2002), etc. It is believed that single WR and OB stars emit soft X-rays ($kT < 1$ keV) via shocks that are set up by instabilities in their supersonic line-driven winds (Lucy & White 1980; Lucy 1982; Owocki et al. 1988). Gräfener & Hamann (2005) have shown that winds of WR stars can be driven by radiation pressure alone if multi-scattering effects are taken into account.

WR 25 (=HD 93162) is a bright ($V \sim 8.03$ mag) WR binary located in the Carina Nebula region. WR 25 is classified as WN6h + O4f (van der Hucht 2001). Gamen et al. (2006) detected periodic radial velocity variations in WR 25 and suggested that WR 25 is an eccentric binary system with a probable period of about 208 days. The basic parameters of WR 25 are summarized in Table 1. The origin of the large X-ray flux of WR 25 is suggestive of colliding wind emission in a binary system (Pollock 1987; Raassen et al. 2003; Pollock & Corcoran 2006). The X-ray to bolometric luminosity ($L_X/L_{\rm bol}$) ratio of $\sim 10^{-5.7}$ (Seward & Chlebowski 1982) for WR 25 is an order of magnitude higher than those observed for single massive stars. Raassen et al. (2003) noticed that the X-ray luminosity of WR 25 had remained relatively constant over a time span of 10 yr. Later, Pollock & Corcoran (2006) found an increase in X-ray luminosity of more than a factor of two and suggested that the observed X-ray variability is a result of colliding wind emission in a moderate eccentric binary. In this context, we use the full set of archival *XMM-Newton* and *Swift* X-ray observations of WR25 to further investigate the properties of the colliding winds in this system. Our aim also extends to search for variability in the

Table 1
Basic Parameters of WR+O Binary, WR 25

Parameters	Value	Ref.[a]	Parameters	Value	Ref.[a]
Period (days)	207.85 ± 0.02	1	v_∞ (km s^{-1})	2480	2
e ($^\circ$)	0.50 ± 0.02	1	$\dot{M}$ ($M_\odot$ yr^{-1})	$10^{-4.3}$	2
V_0 (km s^{-1})	-34.6 ± 0.5	1	Dist. (kpc)	3.24	3
K (km s^{-1})	44 ± 2	1	$L_\star$ ($L_\odot$)	$10^{6.2}$	2
ω ($^\circ$)	215 ± 3	1	$E(B-V)$ (mag)	0.63 mag	3
T_0 (HJD)	2451598 ± 1	1	$L_X/L_{\rm bol}$	10^{-4}	4
$a \sin i$ ($R_\odot$)	156 ± 8	1			

Notes. Here: e is eccentricity, V_0 is radial velocity, K is radial velocity amplitude, ω is the orientation of periastron, T_0 is the Julian date of periastron passage, $a \sin i$ is the semi major axis, v_∞ is the terminal velocity, and $\dot{M}$ is the mass loss rate.
[a] **References.** (1) Gamen et al. 2006; (2) Crowther & Dessart 1998; (3) van der Hucht 2001; (4) Seward & Chlebowski 1982.

V band using the All Sky Automated Survey (ASAS; Pojmanski 2002) archival data.

The paper is organized along the following lines: Section 2 describes the observations and data reduction. The light curve analysis is given in Section 3, X-ray spectral properties of WR 25 are described in Section 4. Section 5 describes the *V*-band optical observations. In Section 6, we present the discussion and conclusions.

2. OBSERVATIONS AND DATA REDUCTION

2.1. XMM-Newton

WR 25 was observed with the *XMM-Newton* satellite using various detector configurations on 20 occasions from the year 2000 to 2009, spanning ~8.5 yr. The *XMM-Newton* satellite is composed of three coaligned X-Ray Telescopes (XRTs; Jansen et al. 2001), which simultaneously observe a source, accumulating photons in three CCD-based instruments, namely the nearly identical MOS1 and MOS2 (Turner et al. 2001) detectors and the PN (Strüder et al. 2001) detectors, which comprise the European Photon Imaging Camera (EPIC). The EPIC instrument provides imaging and spectroscopy in the energy range from 0.15 to 15 keV with an angular resolution of 4.5–6.6 arcsec and a spectral resolution ($E/\Delta E$) of 20–50. Exposure times for these observations were in the range of 6–60 ks. A log of observations is provided in Table 2.

The data were reduced with standard *XMM-Newton* Science Analysis System (SAS) software, version 12.0 using version 3.1 calibration files. The pipeline processing of raw EPIC Observation Data Files was done using the EPCHAIN and EMCHAIN tasks which allow calibrations both in energy and astrometry of the events registered in each CCD chip. We have restricted our analysis to the energy band 0.5–10.0 keV as the background contribution is particularly relevant at high energies where stellar sources have very little flux and are often undetectable. Event list files were extracted using the SAS task EVSELECT. The EPATPLOT task was used for checking for pile-up effects and no observations were affected by pile-up. Data from the three cameras were individually screened for the time intervals with high background. The observations affected by high background flaring events were excluded (see Table 2). X-ray light curves and spectra of WR 25 were generated from on-source counts obtained from circular regions with a radius of 30″ around the source. The background was chosen from several source-free regions on the detectors surrounding the source. We used the tool EPICLCCORR to correct for good time intervals, dead time, exposure, point-spread function, quantum efficiency, and background subtraction. The SAS task ESPECGET was used to generate the spectra, which also computes the photon redistribution as well as the ancillary matrix. Finally, the spectra were rebinned to have at least 20 counts per spectral bin.

2.2. SWIFT

WR 25 has also been regularly monitored by the *Swift* XRT since 2007 November. The XRT observes from 0.3 to 10 keV using CCD detectors, with an energy resolution of ≈140 eV at ~6 keV (Burrows et al. 2005). The exposure times for the XRT observations varied from 1 to 26 ks. All XRT data were collected in photon counting mode. A log of observations is given in Table 3. We have excluded observations with exposure times less than 2 ks due to poor or no signal. In order to produce the cleaned and calibrated event files, all the data were reduced using the *Swift* XRTPIPELINE task (version 0.12.6) in which standard event grades of 0–12 were selected, and calibration files were used from the CALDB 2.8 release.[1]

For every observation, images, light curves, and spectra were obtained with the XSELECT (version 2.4) package. For each observation, source spectra and light curves were extracted from a circular region with a radius of 30″. For the background estimation, an annular region with inner and outer radii of 69″ and 127″ were used around the source region. The spectra were grouped to have a minimum of twenty counts per energy bin with GRPPHA. The spectra were corrected for the fractional exposure loss due to bad columns on the CCD. For this, we created exposure maps with the XRTEXPOMAP task, which is used as an input to generate the ARF with the XRTMKARF task. For the RMF, the latest version was used from the HEASARC calibration database.

2.3. ASAS V-band Observations

WR 25 was observed from 2000 December 3 to 2009 December 3 by ASAS.[2] We have used only "A" and "B" grade data within 1 arcsec to the target of WR 25. ASAS photometry provides five sets of magnitudes corresponding to five aperture values varying in size from 2 to 6 pixels in diameter. For bright objects, Pojmanski (2002) suggested that the magnitudes corresponding to the largest aperture (i.e., the aperture diameter of 6 pixels) are useful. Therefore, we took magnitudes corresponding to the largest aperture for further analysis.

3. X-RAY LIGHT CURVES AND PERIOD ANALYSIS

The background-subtracted X-ray light curves as observed from *XMM-Newton*-EPIC, and *Swift*-XRT in the total (0.5–10.0 keV), hard (2.0–10.0 keV) and soft (0.5–2.0 keV) energy bands are shown in Figures 1(a) and (b), respectively, running from top to bottom. The light curves were binned at 2000 s intervals. The variability in each band is clearly seen. For additional confirmation of the variability in all bands, the significance of deviations from the mean count rate were measured using the χ^2 test, defined as

$$\chi^2 = \sum_{i=1}^{N} \frac{(C_i - \overline{C})^2}{\sigma_i^2}, \quad (1)$$

[1] http://heasarc.gsfc.nasa.gov/docs/heasarc/caldb/caldb_intro.html
[2] http://www.astrouw.edu.pl/asas

Table 2
Log of Observations of WR 25 from *XMM-Newton*

Data Set	Rev.	Observation ID	Detector[1] (Filter[2])	Obs. Date (YYYY-MM-DD)	U.T.[3] (hh:mm:ss)	Exposure Time (s)	Bkg Flare[4] from–to (ks)	Effective Exposure (s)	Off Axis (′)
x01	115	0112580601[5]	M1(TH)	2000 Jul 26	05:07:47	33589	32.8–33.6	32761	6.864
			M2(TH)		06:00:45	30488	29.6–30.5	29585	
			PN(TH)		05:48:51	31198	30.3–31.2	30298	
x02	116	0112580701[5]	M1(TH)	2000 Jul 27	23:57:54	10991	...	10991	6.877
			M2(TH)	2000 Jul 28	00:50:51	7991	...	7991	
			PN(TH)	2000 Jul 28	00:38:57	8999	...	8999	
x03	283	0112560101[5]	M1(TH)	2001 Jun 25	07:34:37	34249	0–9.6	24681	0.066
			M2(TH)		07:40:30	33894	0–9.6	24325	
			PN(TH)		06:51:26	33133	0–8.7	24433	
x04	284	0112560201[5]	M1(TH)	2001 Jun 28	07:29:20	35886	30.0–35.9	30000	0.094
			M2(TH)		07:29:20	35890	30.0–35.9	30000	
			PN(TH)		07:22:56	37364	27.7–37.4	27733	
x05	285	0112560301[5]	M1(TH)	2001 Jun 30	04:45:30	37107	33.6–37.1	33636	0.066
			M2(TH)		04:45:28	37108	33.6–37.1	33636	
			PN(TH)		05:23:05	34526	31.4–34.5	31381	
x06	573	0145740101[6]	M1(TH)	2003 Jan 25	12:58:20	6812	...	6812	7.912
			M2(TH)		12:58:20	6813	...	6813	
x07	574	0145740201[6]	M1(TH)	2003 Jan 27	01:03:43	6961	...	6961	7.855
			M2(TH)		01:03:43	6961	...	6961	
x08	574	0145740301[6]	M1(TH)	2003 Jan 27	20:37:04	6812	...	6812	7.856
			M2(TH)		20:37:05	6812	...	6812	
x09	575	0145740401[6]	M1(TH)	2003 Jan 29	01:40:32	8311	...	8311	7.824
			M2(TH)		01:40:33	8311	...	8311	
x10	575	0145740501[6]	M1(TH)	2003 Jan 29	23:55:06	6811	...	6811	7.815
			M2(TH)		23:55:07	6811	...	6811	
x11	640	0160160101[7]	M1(TH)	2003 Jun 8	13:30:32	28415	0–1.4, 8.9–10.3, 15.5–28.4	12735	5.965
			M2(TH)		13:30:22	28414	as above	12735	
x12	662	0145780101[6]	M1(TH)	2003 Jul 22	01:51:36	8300	...	8300	6.335
			M2(ME)		01:51:29	8300	...	8300	
x13	668	0160560101[6]	M1(TH)	2003 Aug 2	21:01:14	17649	4.7–13.7	8649	6.516
			M2(ME)		21:01:03	17667	4.7–13.7	8649	
x14	671	0160560201[6]	M1(TH)	2003 Aug 9	01:44:20	12652	9.5–10.3	11863	6.557
			M2(ME)		01:44:08	12652	9.5–10.3	11863	
x15	676	0160560301[6]	M1(TH)	2003 Aug 18	15:23:34	18850	...	18850	7.070
			M2(ME)		15:23:22	18850	...	18850	
x16	1126	0311990101[7]	M1(TH)	2006 Jan 31	18:04:22	63034	...	63034	7.656
			M2(TH)		18:04:20	66036	...	66036	
			PN(TH)		18:26:30	30000	0–3.0	26961	
x17	1662	0560580101[8]	M1(TH)	2009 Jan 5	10:23:02	14602	...	14602	8.025
			M2(TH)		10:22:53	14602	...	14602	
x18	1664	0560580201[8]	M1(TH)	2009 Jan 9	14:28:07	11603	...	11603	7.999
			M2(TH)		14:27:58	11603	...	11603	
x19	1667	0560580301[8]	M1(TH)	2009 Jan 15	11:22:56	26552	...	26552	7.942
			M2(TH)		11:22:46	26552	...	26552	
x20	1676	0560580401[8]	M1(TH)	2009 Feb 2	05:31:18	23903	...	23903	7.757
			M2(TH)		04:46:09	26613	...	26613	
			PN(TH)		04:45:24	24669	...	24669	

Notes. [1] M1 and M2 stand for MOS1 and MOS2, respectively. [2] TH and ME stand for thick and medium filters, respectively. [3] Exposure start time. [4] Background proton flare duration during the observations. PIs of observations were [5] Dr. Albert Brinkman, [6] Dr. Michael Corcoran, [7] Dr. Fred Jansen, and [8] Dr. Kenji Hamaguchi.

where $\overline{C}$ is the average count rate, C_i is the count rate of ith observations, and σ_i is the error corresponding to C_i. The χ^2 statistic was compared against a critical value (χ^2_ν) for 99.9% significance level, obtained from the χ^2-probability function. For the *XMM-Newton* MOS light curves, χ^2 values were obtained to be 6440, 4403, and 4499 in the total, hard and soft bands, respectively. These values of χ^2 are very large in comparison to the χ^2_ν of 1430 for 1599 degrees of freedom. For *Swift*-XRT light curves in total, hard and soft bands, χ^2 values of 5188, 5113, and 5124 were obtained, respectively, with $\chi^2_\nu =$ 393 for 483 degrees of freedom. This indicates that WR 25 is essentially variable in all X-ray bands.

The present long-term X-ray data as observed from *XMM-Newton* permit us to derive the orbital period of WR 25. We have performed a period analysis of light curves in all bands with a Lomb–Scargle periodogram (Lomb 1976; Scargle 1982). The plots from top to bottom in Figure 2 show the power spectra in the total, hard and soft bands, respectively. The frequency corresponding to the highest peak was found to be 0.00482 ± 0.00008 cycles day^{-1} in all bands. Other

Table 3
Log of Observations of WR 25 from *Swift*

Set	Observation ID	Obs. Date (YY-MM-DD)	U. T. (hh:mm:ss)	Exposure Time(s)	Offset (′)
s01	00037049001[1]	2007 Dec 11	14:09:00	4490.5	6.339
s02	00037049002[1]	2008 Jan 19	06:08:01	3246.6	4.682
s03	00031097001[2]	2008 Jan 25	02:00:01	4440.5	1.342
s04	00031097002[2]	2008 Jan 26	02:10:01	3717.2	0.387
s05	00031097003[2]	2008 Jan 27	00:44:00	3452.8	3.892
s06	00031097004[2]	2008 Jan 28	00:57:00	3787.7	0.584
s07	00031097006[2]	2008 Jan 30	17:18:01	3876.7	0.803
s08	00031097007[2]	2008 Jan 31	06:17:01	2585.1	1.518
s09	00031097008[2]	2008 Feb 1	00:04:00	26394.8	0.182
s10	00031097009[2]	2008 Feb 2	23:59:01	22568.9	0.999
s11	00031097010[2]	2008 Feb 5	16:40:01	3468.7	1.396
s12	00031097011[2]	2008 Feb 6	00:27:26	3332.3	3.913
s13	00031097012[2]	2008 Feb 7	00:34:46	3372.7	1.334
s14	00031097013[2]	2008 Feb 9	21:33:01	2785.1	0.923
s15	00031097016[2]	2008 Feb 11	17:02:01	2478.9	2.168
s16	00031097017[2]	2008 Feb 12	00:45:01	2967.9	1.300
s17	00031097018[2]	2008 Feb 13	07:15:01	2598.9	1.590
s18	00031097019[2]	2008 Feb 14	15:22:01	3382.0	0.412
s19	00031097020[2]	2008 Feb 15	12:29:01	2422.4	1.264
s20	00031097022[2]	2008 Feb 17	12:52:01	3692.9	3.464
s21	00031097023[2]	2008 Feb 18	17:30:00	3389.9	1.234
s22	00031097025[2]	2008 Feb 20	06:15:01	3392.9	2.647
s23	00031097026[2]	2008 Feb 21	07:57:01	3646.4	2.027
s24	00031097028[2]	2008 Feb 23	14:33:01	2977.3	1.415
s25	00031097029[2]	2008 Feb 24	16:14:00	2349.4	0.638
s26	00031097030[2]	2008 Feb 25	11:35:01	2408.8	0.816
s27	00031097031[2]	2008 Feb 26	05:10:01	3835.2	2.159
s28	00031097034[2]	2008 Mar 16	08:35:01	9246.5	1.688
s29	00031308001[3]	2008 Dec 14	03:17:01	6758.9	6.929
s30	00090033001[4]	2009 Mar 18	08:44:01	14363.4	6.457
s31	00031097035[2]	2009 Apr 1	12:10:22	9225.9	1.270
s32	00031097036[2]	2009 Apr 2	08:59:01	12517.4	1.741
s33	00031097037[2]	2009 Apr 3	09:10:01	10208.9	1.064
s34	00031097038[2]	2009 Apr 7	09:24:01	8674.8	0.911
s35	00031097039[2]	2009 Apr 8	07:53:01	8259.7	1.191
s36	00031097040[2]	2009 Apr 9	13:04:00	9845.3	1.465
s37	00031097041[2]	2009 Jun 3	01:46:01	3790.9	0.348
s38	00031097042[2]	2009 Jun 4	06:51:00	3923.2	1.858
s39	00031097043[2]	2009 Jun 5	06:58:00	3364.8	1.595
s40	00031097044[2]	2009 Jun 6	06:50:01	4194.7	3.771

Notes. Proposers of observations were [1]F. Senziani, [2]A. Pollock, [3]E. Pian, and [4]M. Corcoran.

frequencies were also noticed in the power spectra but are not consistent with each other among all the energy bands. Thus, the corresponding period of 207.5 ± 3.4 days appears to be real. Also, the derived period is very similar to the orbital period ($=207.85 \pm 0.02$ days) derived by Gamen et al. (2006) using radial velocity measurements.

Further, the X-ray light curves as observed from *XMM-Newton*-MOS and *Swift*-XRT in the total, hard and soft energy bands were folded using the ephemeris HJD = 2,451,958.0 + 207.85E (Gamen et al. 2006) and are shown in Figures 3(a) and (b), respectively. The zero phase in the folded light curves corresponds to the time of periastron (HJD 2,451,958.0). X-ray light curves in each band from both observations show similar behavior. The light curves in the individual bands show phase-locked variability. In the soft- and total-band light curves, the count rates decrease when going from orbital phase 0.0 (i.e., near the periastron passage) to orbital phase ∼0.03, then increase up to phase ∼0.2. Count rates further decrease to phase ∼0.7 before reaching a maximum value near periastron passage. However, in the hard band, the count rates were systematically decreasing when going from periastron to apastron. The ratio of maximum to minimum count rates in total, soft, and hard bands were found to be 1.9, 2.6, and 1.7 for *XMM-Newton*-MOS observations, and 2.5, 2.6, and 2.9 for *Swift*-XRT observations, respectively.

The hardness ratio (HR) defined as (Hard–Soft)/(Hard+Soft) can reveal information about the spectral variations. The HR curve displayed in plot (d) of Figure 3 exhibits similar behavior to that of the light curves in the hard band. The maximum value of the HR during periastron passage indicates a harder spectrum.

4. X-RAY SPECTRAL ANALYSIS

X-ray spectra of WR 25 as observed by the EPIC detector of *XMM-Newton* at different orbital phases are shown in Figure 4. Below 1 keV, the X-ray spectra were found to be affected by high extinction. Strong emission lines like Fe XVII (0.8 keV), Ne X (1.02 keV), Mg XII (1.47 keV), Si XIII (1.853 keV), S XV (2.45 keV), Ar XVII (3.12 keV), Ca XIX+XX (3.9 keV), and Fe XXV (6.67 keV) were identified in the X-ray spectra of WR 25. In order to derive the spectral parameters at different orbital phases, we performed spectral analysis of each data set corresponding to different orbital phases using simultaneous/joint fitting of EPIC data by models of the Astrophysical Plasma Emission Code (APEC; Smith et al. 2001), as implemented in the X-ray spectral fitting package XSPEC (Arnaud 1996) version 12.7.1. For spectral fitting, we adopted the similar approach of Raassen et al. (2003) and Pollock & Corcoran (2006). The form of the model used was WABS(ISM)*WABS(LOCAL)*(VAPEC+VAPEC). A χ^2 minimization gave the best fit model to the data. The presence of interstellar material along the line of sight and the local circumstellar material around the stars can modify the X-ray emission from massive stars. We have applied the local absorption in the line of sight to the source using photoelectric absorption cross-sections according to Morrison & McCammon (1983) and modeled as WABS with two absorption components, i.e., interstellar medium ($N_{\rm H}^{\rm ISM}$) and local ($N_{\rm H}^{\rm local}$) hydrogen column densities. Assuming the $E(B-V) \sim 0.63$ mag (van der Hucht 2001) and a normal interstellar reddening law toward WR 25, and using the relation given by Gorenstein (1975), the $N_{\rm H}^{\rm ISM}$ was estimated to be $\sim 3.7 \times 10^{21}$ cm^{-2}. For the first stage of spectral fitting, we fixed the $N_{\rm H}^{\rm ISM}$ and abundances of He(=2.27), C(=0.15), and N(=5.9), and varied other parameters for all phases. The values of He, C, and N abundances were adopted from the optical spectrum of WR 25 (Crowther et al. 1995). The temperatures for both components were found to be constant within the 1σ level at all phases. However, abundances of Ne, Mg, Al, Si, Ca, Ar, Fe, and Ni were found to be constant within the 1–2σ level. Average values of elemental abundances and temperatures are given in Table 4. In the next stage of spectral fitting, we fixed temperatures and abundances of all elements at their average values for all phases along with $N_{\rm H}^{\rm ISM}$, and varied $N_{\rm H}^{\rm local}$ and normalizations of both components. Many spectra were taken at the same orbital phase; therefore, joint spectral fittings were performed for those spectra, which were observed within a difference of $\leqslant 0.02$ in the orbital phase. In this way, from *XMM-Newton* observations, we have nine data points over an orbital cycle of WR 25. The final set of the best-fitted parameters is given in Table 5.

The method used for the fitting of *XMM-Newton*-EPIC spectra was also applied for the fitting of spectra observed from the *Swift*-XRT. Since WR 25 was observed more than 40 times

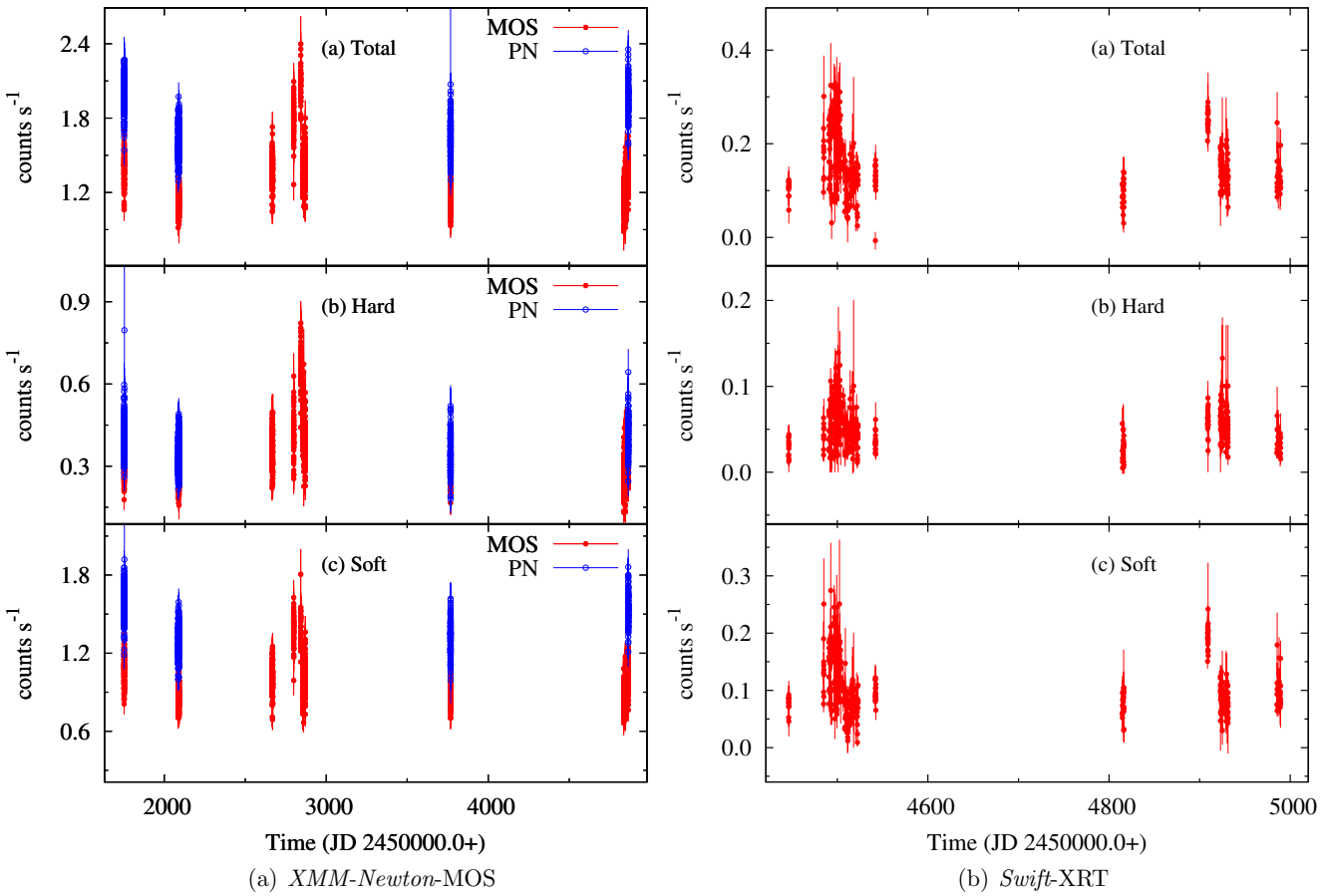

Figure 1. X-ray light curves in total (0.3–10.0 keV), hard (2.0–10.0 keV), and soft (0.3–2.0 keV) energy bands as observed from (a) *XMM-Newton*-EPIC and (b) *Swift*-XRT.

(A color version of this figure is available in the online journal.)

Table 4
Average Values of Temperatures and Abundances of WR 25 as Obtained from X-Ray Spectral Fitting

Parameters	Value	Parameters	Value
kT_1 (keV)	$0.628^{+0.009}_{-0.007}$	Si	$1.07^{+0.09}_{-0.07}$
kT_2 (keV)	$2.75^{+0.06}_{-0.05}$	S	$1.59^{+0.11}_{-0.10}$
O	<0.1	Ar	$1.30^{+0.27}_{-0.22}$
Ne	$1.60^{+0.19}_{-0.14}$	Ca	$1.67^{+0.42}_{-0.38}$
Mg	$1.38^{+0.12}_{-0.09}$	Fe	$0.68^{+0.05}_{-0.04}$
Al	$4.42^{+1.28}_{-0.86}$	Ni	$3.93^{+0.81}_{-0.68}$

Note. Abundances are in units of solar photospheric values.

by the *Swift*-XRT and many observations were taken with short exposures, the spectra with a phase difference of $\leqslant 0.02$ were fitted jointly. In this way, we have spectra at 12 different phases over an orbital cycle from *Swift* observations. For the spectral fitting of *Swift*-XRT data, we have fixed temperatures and abundances to values as obtained from spectral fitting of *XMM-Newton*-EPIC data. However, $N_{\rm H}^{\rm local}$ and normalizations of both components were kept as free parameters in the spectral fitting. The best fit parameters from the spectral fitting of *Swift*-XRT data are also given in Table 5. We have compared various parameters derived from both *observatories*. It appears that the X-ray fluxes and other spectral parameters derived from spectral fitting of both satellite data are consistent. Comparison of spectral parameters derived from both telescopes may not be possible due to the lack of simultaneous observations. However, Plucinsky et al. (2012) has shown that the spectral parameters from both observations are in agreement within ±10%.

The X-ray fluxes of WR 25 are estimated using the CFLUX model in XSPEC and are corrected for $N_{\rm H}^{\rm ISM}$. The X-ray luminosities of WR 25 in soft (L_{Xs}), hard (L_{Xh}), and total (L_{Xt}) energy bands were derived by using the corresponding unabsorbed flux values and a distance of 3.24 kpc. The emission measures (EMs), EM_1 and EM_2, corresponding to both the cool and the hot plasma components are derived from the normalization parameters. We have plotted L_{Xs}, L_{Xh}, L_{Xt}, $N_{\rm H}^{\rm local}$, EM_1, and EM_2 as a function of orbital phase in Figures 5(a) and (b) for observations from *XMM-Newton* and *Swift*, respectively. The maximum value of L_{Xs} was found near periastron passage and dropped suddenly to phase ∼0.03 and then increased to phase ∼0.3. After phase ∼0.3, L_{Xs} decreased to phase ∼0.7. It appears that L_{Xs} peaked twice during an orbital cycle. The minimum value L_{Xs} was observed just after periastron passage, which was ∼3.2 times lower than the observed maximum value. A similar tendency of X-ray luminosity was also observed in the total energy band, where the maximum to minimum flux ratio was found to be ∼2.3. Apart from the periastron passage, no other peak of L_{Xh} was noticed in an orbital cycle of WR 25. The minimum value of L_{Xh} was observed near phase ∼0.5 and was ∼3.1 times lower than that observed during the periastron passage. The value of $N_{\rm H}^{\rm local}$ was observed to be maximum after the periastron passage at phase 0.03. However, the minimum value of $N_{\rm H}^{\rm local}$ was observed at phase ∼0.5. The EMs, EM_1 and EM_2, corresponding to the

Table 5
Best Fit Parameters Obtained from X-Ray Spectral Fitting of WR 25

Set	Phase	$N_{\rm H}^{\rm local}$	$\rm EM_1$	$\rm EM_2$	L_{Xs}	L_{Xh}	L_{Xt}	χ^2_ν(dof)				
					XMM							
1	x13,x14	x06,x07,x08, x09,x10,x15	x03,x04,x05	x16	x17	x18,x19	x01,x02,x20	x11	x12	...	...	...
2	0.060	0.141	0.360	0.438	0.583	0.617	0.735	0.779	0.988	...	...	...
3	$0.62^{+0.03}_{-0.03}$	$0.45^{+0.01}_{-0.02}$	$0.34^{+0.01}_{-0.01}$	$0.32^{+0.01}_{-0.01}$	$0.29^{+0.03}_{-0.04}$	$0.28^{+0.02}_{-0.02}$	$0.32^{+0.01}_{-0.01}$	$0.29^{+0.03}_{-0.03}$	$0.68^{+0.04}_{-0.04}$	...	...	...
4	$6.25^{+0.61}_{-0.61}$	$6.72^{+0.35}_{-0.35}$	$5.27^{+0.12}_{-0.12}$	$5.00^{+0.20}_{-0.20}$	$4.20^{+0.53}_{-0.52}$	$4.47^{+0.35}_{-0.34}$	$5.89^{+0.17}_{-0.17}$	$5.42^{+0.53}_{-0.52}$	$12.77^{+1.39}_{-1.36}$	...	...	...
5	$5.45^{+0.14}_{-0.14}$	$4.03^{+0.09}_{-0.09}$	$2.87^{+0.03}_{-0.03}$	$2.97^{+0.06}_{-0.06}$	$2.80^{+0.15}_{-0.15}$	$3.36^{+0.10}_{-0.10}$	$3.46^{+0.05}_{-0.05}$	$3.36^{+0.16}_{-0.16}$	$7.73^{+0.31}_{-0.32}$	...	...	...
6	$4.82^{+0.06}_{-0.06}$	$6.33^{+0.06}_{-0.06}$	$6.22^{+0.09}_{-0.06}$	$6.22^{+0.17}_{-0.06}$	$5.84^{+0.12}_{-0.12}$	$6.62^{+0.08}_{-0.07}$	$7.42^{+0.19}_{-0.07}$	$7.40^{+0.13}_{-0.13}$	$7.86^{+0.14}_{-0.14}$	...	...	...
7	$4.91^{+0.06}_{-0.06}$	$3.87^{+0.03}_{-0.03}$	$2.80^{+0.07}_{-0.01}$	$2.85^{+0.10}_{-0.05}$	$2.72^{+0.05}_{-0.06}$	$3.22^{+0.04}_{-0.04}$	$3.35^{+0.11}_{-0.06}$	$3.29^{+0.06}_{-0.06}$	$7.18^{+0.13}_{-0.12}$	...	...	...
8	$9.74^{+0.12}_{-0.12}$	$10.20^{+0.09}_{-0.09}$	$9.03^{+0.14}_{-0.02}$	$9.08^{+0.27}_{-0.11}$	$8.56^{+0.17}_{-0.18}$	$9.84^{+0.11}_{-0.11}$	$10.77^{+0.30}_{-0.13}$	$10.69^{+0.18}_{-0.18}$	$15.04^{+0.26}_{-0.26}$	...	...	...
9	1.18(598)	1.07(1048)	1.23(2956)	1.32(965)	1.37(227)	1.12(554)	1.30(2336)	1.28(270)	1.25(281)	...	...	...
					Swift							
1	s15,s16,s17, s32,s33	s19,s20,s21, s34,s35,s36	s22,s23,s24, s25,s26,s27	s28	s37,s38,s39, s40	s29	s01	s02	s03,s04,s05, s06,s30	ss07,s08 s09,s10	s11, s12 s13	s14, s31
2	0.009	0.028	0.057	0.163	0.306	0.476	0.70 3	0.889	0.924	0.952	0.975	0.995
3	$0.98^{+0.11}_{-0.11}$	$1.09^{+0.13}_{-0.12}$	$0.99^{+0.19}_{-0.18}$	$0.52^{+0.14}_{-0.14}$	$0.32^{+0.12}_{-0.12}$	$0.23^{+0.18}_{-0.21}$	$0.46^{+0.11}_{-0.09}$	$0.40^{+0.20}_{-0.22}$	$0.40^{+0.17}_{-0.18}$	$0.54^{+0.05}_{-0.05}$	$0.56^{+0.14}_{-0.15}$	$0.77^{+0.17}_{-0.18}$
4	$13.04^{+2.43}_{-2.29}$	$13.37^{+2.59}_{-2.39}$	$12.72^{+3.66}_{-3.27}$	$8.22^{+2.46}_{-2.34}$	$6.34^{+1.85}_{-1.82}$	$4.90^{+2.38}_{-2.27}$	$7.18^{+1.55}_{-1.55}$	$11.86^{+5.33}_{-5.18}$	$13.19^{+5.20}_{-4.97}$	$14.57^{+1.41}_{-1.38}$	$11.25^{+3.85}_{-3.76}$	$10.73^{+3.92}_{-3.67}$
5	$5.34^{+0.39}_{-0.39}$	$5.01^{+0.36}_{-0.37}$	$4.21^{+0.50}_{-0.51}$	$3.22^{+0.54}_{-0.55}$	$2.96^{+0.44}_{-0.45}$	$2.32^{+0.61}_{-0.64}$	$3.13^{+0.71}_{-0.71}$	$4.59^{+1.18}_{-1.19}$	$5.89^{+1.19}_{-1.21}$	$6.69^{+0.30}_{-0.30}$	$7.74^{+0.74}_{-0.75}$	$7.11^{+0.65}_{-0.66}$
6	$4.45^{+0.14}_{-0.14}$	$3.85^{+0.12}_{-0.12}$	$4.11^{+0.19}_{-0.19}$	$6.13^{+0.39}_{-0.39}$	$7.76^{+0.40}_{-0.40}$	$7.47^{+0.64}_{-0.64}$	$6.05^{+0.57}_{-0.57}$	$11.48^{+1.02}_{-1.02}$	$13.14^{+0.96}_{-0.96}$	$10.82^{+0.20}_{-0.20}$	$9.04^{+0.40}_{-0.40}$	$5.87^{+0.26}_{-0.26}$
7	$5.03^{+0.16}_{-0.16}$	$4.72^{+0.15}_{-0.15}$	$4.12^{+0.19}_{-0.19}$	$3.27^{+0.21}_{-0.21}$	$3.01^{+0.15}_{-0.15}$	$2.38^{+0.20}_{-0.20}$	$3.07^{+0.29}_{-0.29}$	$4.76^{+0.42}_{-0.42}$	$5.95^{+0.44}_{-0.44}$	$6.60^{+0.12}_{-0.12}$	$7.22^{+0.32}_{-0.32}$	$6.47^{+0.29}_{-0.29}$
8	$9.49^{+0.30}_{-0.30}$	$8.57^{+0.27}_{-0.27}$	$8.23^{+0.37}_{-0.37}$	$9.41^{+0.59}_{-0.59}$	$10.77^{+0.55}_{-0.55}$	$9.85^{+0.84}_{-0.84}$	$9.12^{+0.86}_{-0.86}$	$16.23^{+1.45}_{-1.45}$	$19.10^{+1.40}_{-1.40}$	$17.42^{+0.32}_{-0.33}$	$16.26^{+0.72}_{-0.72}$	$12.34^{+0.55}_{-0.56}$
9	1.40 (178)	1.21 (191)	1.15 (103)	1.17(49)	1.12(85)	1.16(31)	1.50(20)	1.11(25)	1.05(93)	1.38 (423)	1.14(92)	1.15 (88)

Notes. $\rm EM_1$ and $\rm EM_2$ are in units of 10^{56} cm^{-3}, $N_{\rm H}^{\rm local}$ is in units of 10^{22} cm^{-2}, and L_{Xs}, L_{Xh}, and L_{Xt} are unabsorbed X-ray luminosities in soft, hard, and total bands in units of 10^{33} erg s^{-1}. Abundances are in units of solar photospheric values. χ^2_ν is χ^2 per degree of freedom and dof is the degree of freedom.

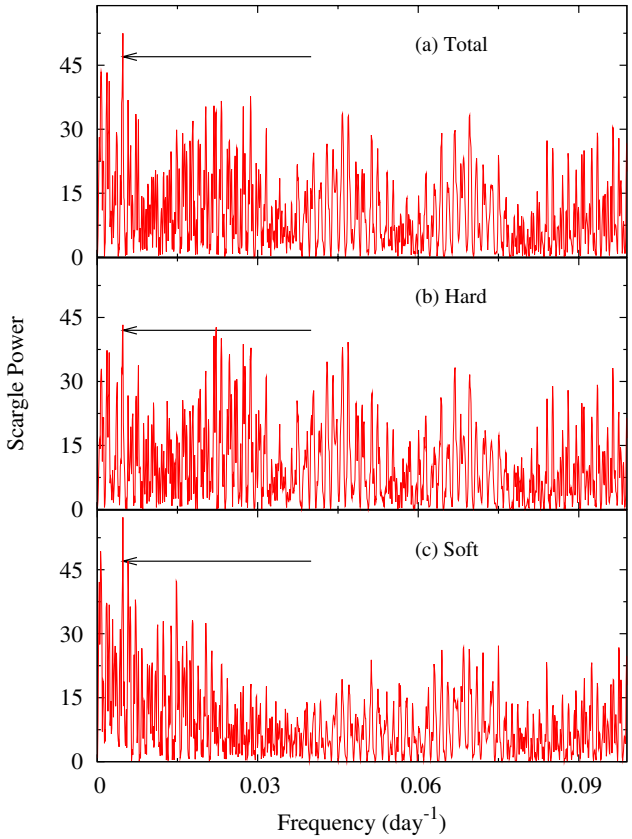

Figure 2. Lomb–Scargle power spectra of X-ray data in different energy bands as observed from EPIC detectors of *XMM-Newton*.

(A color version of this figure is available in the online journal.)

cool and the hot temperature components were also found to be phase dependent, with maximum at periastron passage and minimum at apastron passage.

5. OPTICAL *V*-BAND LIGHT CURVE

The *V*-band light curve of WR 25 as obtained from the ASAS archive is plotted in Figure 6(a). In ASAS observations, error bars are very large (i.e., 0.035–0.1 mag). Therefore, it is difficult to search for any small scale variability that might be present. In order to reduce the short term fluctuations, a moving average of 10 data points in the forward direction was performed. The light curve of the moving-averaged data points is shown in Figure 6(b). The *V*-band light curve does not appear to be constant over the time span of the observations; however, variations are not statistically significant. The χ^2 was found to be 270 for 956 degrees of freedom (see Equation (1)). This value of χ^2 is very low in comparison to the χ^2_ν of 826 corresponding to the 99.9% significance level. Furthermore, we have folded the *V*-band data with phase bins of 0.1 and using the ephemeris given by Gamen et al. (2006). The folded *V*-band light curve of WR 25 is shown in Figure 6(c). It appears that variability is present in the light curve. The variability amplitude was found to be 7.3 ± 0.2 mmag. The maximum brightness was seen near periastron passage and after that the brightness decreased toward apastron passage, being minimum near phase ∼0.75.

6. DISCUSSION AND CONCLUSIONS

We have carried out X-ray and optical studies of WR 25 using X-ray data from the *XMM-Newton* and *Swift* satellites and optical data from the ASAS archive. The X-ray spectra

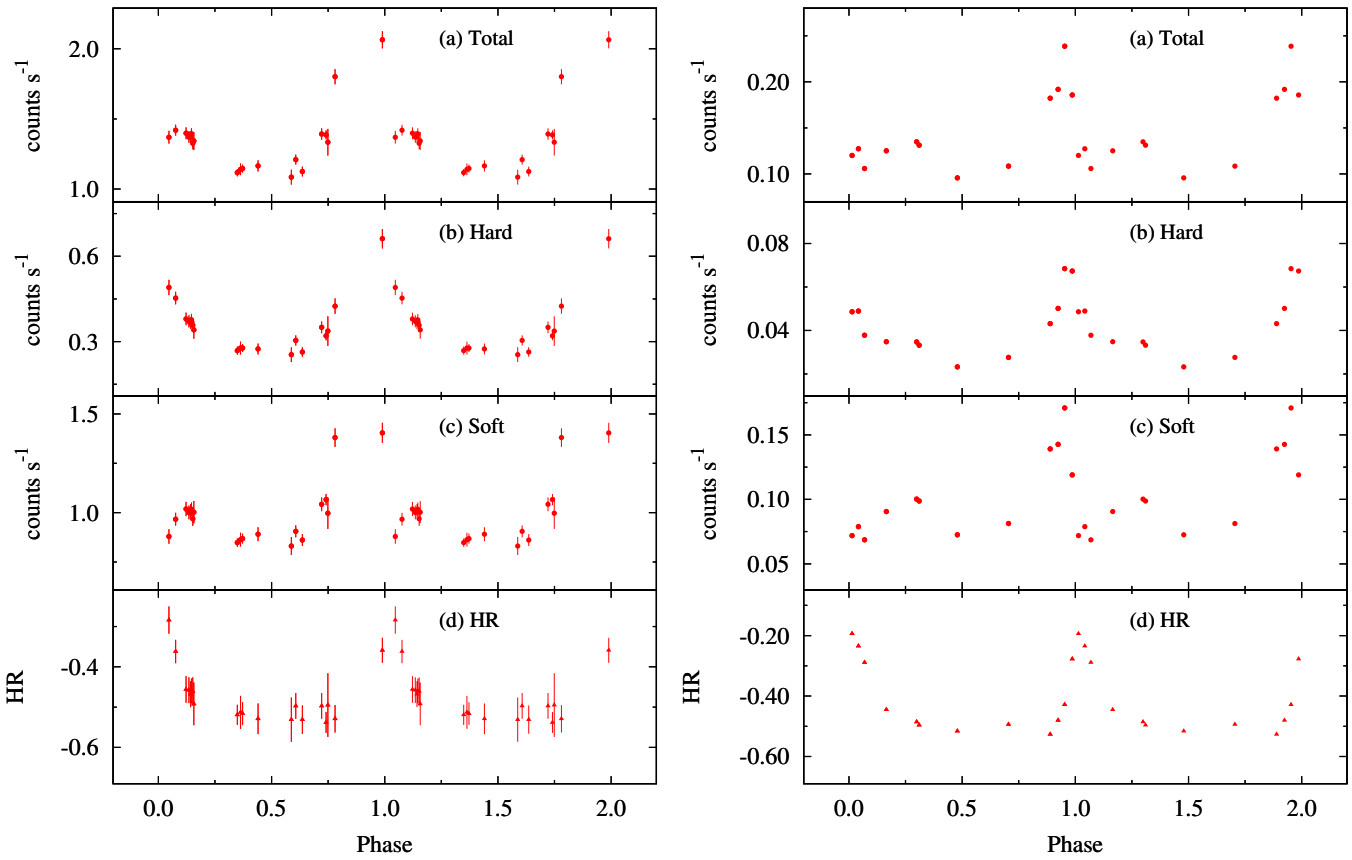

Figure 3. Folded light curves using the ephemeris derived by Gamen et al. (2006) in different energy bands as observed from (a) *XMM-Newton* (b) *Swift*.
(A color version of this figure is available in the online journal.)

of WR 25 at all orbital phases are well-explained by a two-temperature plasma model. The temperatures of both components were found to be constant throughout an orbital cycle. The temperature values are similar to those derived by Pollock & Corcoran (2006) and Raassen et al. (2003) using *XMM-Newton* data. The temperature of the cool component (=0.628 keV) of WR 25 is comparable to that of other WN-subtype WR+O binaries: for example WR1 (0.56–0.67 keV; Ignace et al. 2003), WR 22 (0.6 keV; Gosset et al. 2009) WR 47 (0.57 ± 0.05 keV; Bhatt et al. 2010b), WR 139 (0.63 ± 0.05; Bhatt et al. 2010b), and WR 147 (0.7–0.8 keV; Skinner et al. 2007). A plasma temperature of 0.6–0.8 keV is also dominant for massive OB stars (Sana et al. 2006; Nazé 2009; Bhatt et al. 2010a). The soft X-ray component may originate in the winds of the individual components of WR 25 via radiation-driven instability shocks. The ratio between the wind momentum ($\dot{M}v_\infty$) and the momentum of the radiation field (L/c) for WR 25 was derived to be $\sim$1 (Hamann et al. 2006), indicating that wind of WR 25 is driven by radiation pressure. Furthermore, the derived temperature of the cool component appears to be realistic for radiation-driven wind shocks. The derived plasma temperature for WR 25 can be used to estimate the pre-shock velocity using the relation $kT_{sh} = 1.95\mu v_{1000}^2$ keV (Luo et al. 1990), where μ is mean mass per particle in units of the proton's mass (1.16 for a WN star and 0.62 for an O-type star), and v_{1000} is shock velocity in units of 1000 km s^{-1}. The pre-shock velocities corresponding to the cool temperature for the WN and O components of WR 25 were found to be 527 and 721 km s^{-1}, respectively. These values are about a factor of $\sim$2 more than those predicted by the radiative shock model of Lucy (1982). The advanced version of the wind-shock model by Owocki et al. (1988) predicts X-ray emission up to 1 keV. The hydrodynamic shocks, which are expected to occur within unstable stellar winds of massive O-type stars, also show similar pre-shock velocities (Feldmeier et al. 1997). Observationally some apparently single WN stars (e.g., WR 1, WR 6, and WR 110) show intrinsic X-ray emission (Skinner et al. 2002a, 2002b; Ignace et al. 2003) while apparently single WC stars and the WN-subtype WR star, WR 40, have not been detected in X-rays thus far (Oskinova 2005; Gosset et al. 2005).

The temperature corresponding to the hot plasma of WR 25 is intermediate compared to those observed for other similar WR binaries (Zhekov 2012). Using the mean particle weight for WN stars, the maximum shock temperature on the line of centers for an adiabatic shock corresponds to a pre-shock wind velocity of 1103 ± 12 km s^{-1} (see Luo et al. 1990), which is $\sim$50% of the observed terminal velocity (Crowther & Dessart 1998; Niedzielski & Skorzynski 2002) of WR 25. This could be due to an oblique wind collision over most parts of the shock, which occurs with a lower velocity normal to the shock and thus leads to a lower plasma temperature. The derived values of $N_{\rm H}^{\rm local}$ and X-ray luminosities exhibit phase-related time variability. We found $N_{\rm H}^{\rm local}$ to be maximum after periastron passage and minimum when L_{Xt} is maximum during periastron passage. It also appears that $N_{\rm H}^{\rm local}$ reached a peak value during the eclipse, indicating that the extra absorption could be due to winds from the WN star. The column density along the line of sight through the WR wind to the region of stellar wind collision is $N_{\rm H}^{\rm local} \propto \dot{M}D^{-1}v_\infty^{-1}$ (Usov 1992), where D is the distance

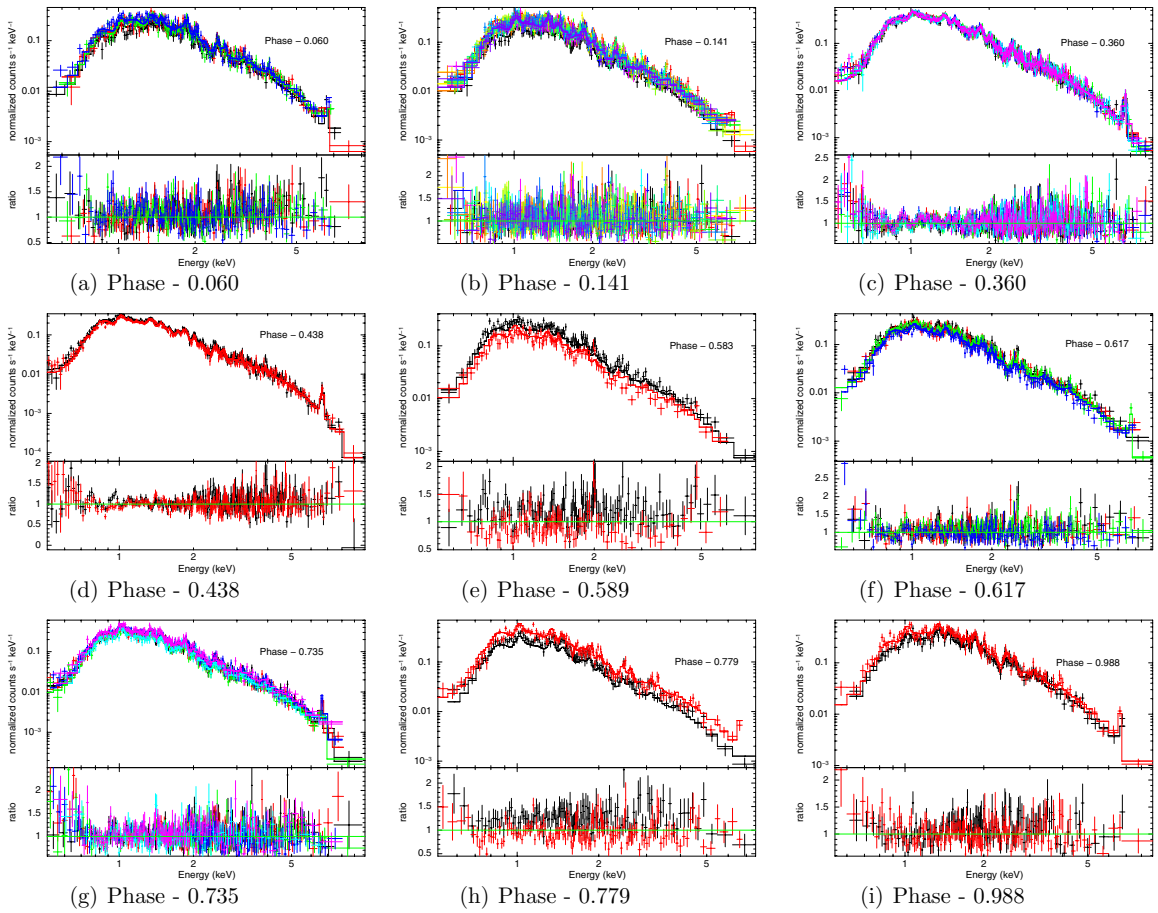

(a) Phase - 0.060 (b) Phase - 0.141 (c) Phase - 0.360

(d) Phase - 0.438 (e) Phase - 0.589 (f) Phase - 0.617

(g) Phase - 0.735 (h) Phase - 0.779 (i) Phase - 0.988

Figure 4. X-ray spectra of WR 25 as observed from MOS and PN detectors along with the best fit folded 2T VAPEC model at nine epochs. WR 25 was observed with the PN detector only at three phases, namely 0.360, 0.438, and 0.735. The PN spectra are shown on the top at these three epochs. The lower panels show the residual in terms of the ratio of the data and model. The emission lines of Ne X, Mg XI+XII, Si III+IV, S XV+XVI, Ar XVII+XVIII, Ca XIX+XX, and Fe (K-shell) are seen in the spectra. (A color version of this figure is available in the online journal.)

between the binary components. Using the parameters of WR 25, $N_{\rm H}^{\rm local}$ was estimated to be $\sim 1.36 \times 10^{22}$ cm^{-2}, which is quite similar to the observed maximum value (see Table 5).

The EMs corresponding to the cool and hot temperatures change substantially, reflecting the variations in X-ray luminosities in the soft and hard bands. The X-ray luminosities observed for WR 25 were found to be more than that for other close WR+O binaries and single WN stars (Zhekov 2012; Skinner et al. 2010). X-ray light curves of WR 25 as observed from *XMM-Newton* and *Swift* show similar behavior. However, in terms of phase coverage, the light curves from *Swift* are much better than those observed from *XMM-Newton*. The deficit in X-ray flux just after periastron passage could be due to the eclipse of the wind interaction zone by the wind of the WN star. In all bands, the excess emission is strongest near periastron passage. The X-ray enhancement after the eclipse in the soft band indicates that besides the colliding wind, individual components of the WR 25 system also contribute to the X-ray emission. The soft X-ray flux peaked near phase 0.5, which further supports that both of the components of WR 25 are sources of soft X-rays, enhancing the combined soft X-ray flux when both of the stars are completely visible to the observer. During phase $\sim$0.7, the soft X-rays further decrease to the minimum value indicating the possibility of a secondary eclipse, when the O star is in front of the primary WN star. The deeper primary eclipse at phase $\sim$0.03 could be due to the larger opacity of the WN wind. On the other hand, L_{Xh} was found to be at minimum during phase $\sim$0.5. Both components of WR 25 are farthest apart at phase 0.5; therefore, the collision is weak, generating fewer X-rays. This indicates that the hard X-rays originate from the collision zone of the wind giving enhanced flux during periastron passage. Stevens et al. (1992) and many other authors showed that strong winds from massive stars collide and generate hard X-rays, in addition to softer X-ray components, due to intrinsic or individual components (Berghoefer et al. 1997; Sana et al. 2006). The phase-locked X-ray variability could be a result of changing separation in an eccentric orbit of WR 25. Figure 7 shows that the X-ray luminosity varies as a function of the inverse binary separation $[1/(D/a)]$. It appears that soft X-ray luminosity does not depend on the binary separation. However, it is clearly seen that the hard X-ray luminosity is linearly dependent on the inverse of the binary separation. The Pearson correlation coefficients for L_{Xs} versus $1/(D/a)$ and L_{Xh} versus $1/(D/a)$ were derived to be -0.02 and 0.87 with a probability of no correlation found to be 0.94 and 10^{-5}, respectively. This indicates that the hard X-rays in WR 25 are due to the collision of winds. The wide massive binary systems whose X-ray luminosities follow the $1/D$ relation are Cyg OB2 # 9 (Nazé et al. 2012) and HD 93205 (Antokhin et al. 2003). Cyg OB2 # 8A and WR140 are the massive binary systems which deviate from expectations at periastron, since the collisions

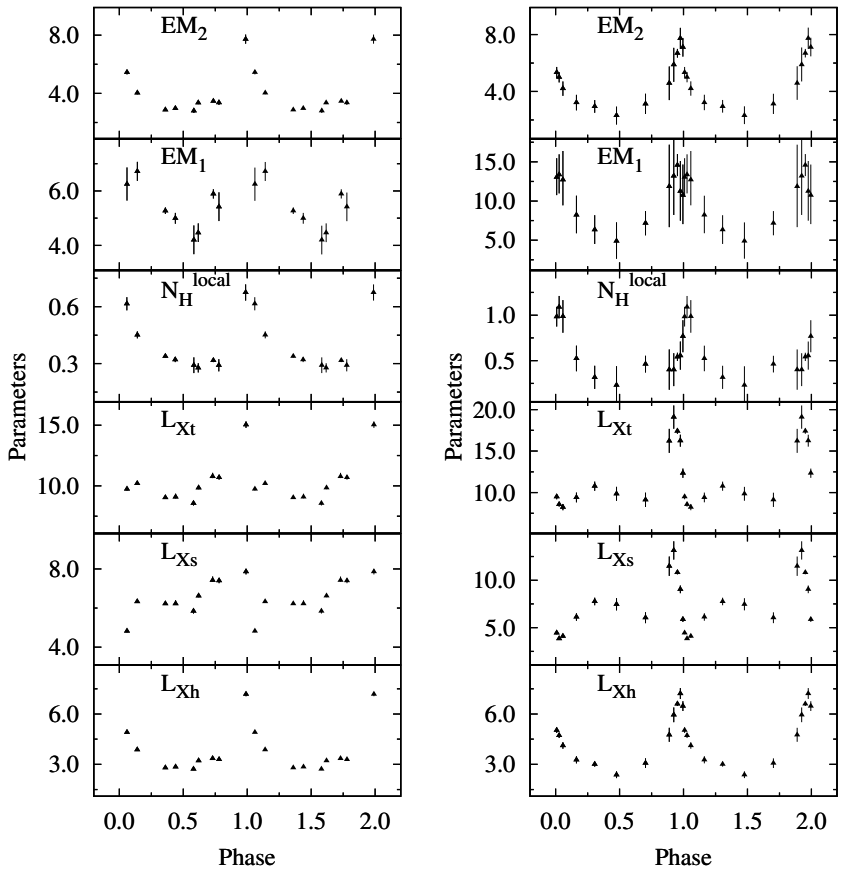

(a) XMM-Newton EPIC observations (b) Swift XRT observations

Figure 5. Spectral parameters as a function of orbital phase as observed from (a) *XMM-Newton*-EPIC and (b) *Swift*-XRT, where X-ray luminosities are in units of 10^{33} erg s^{-1}, $N_{\rm H}^{\rm local}$ is in units of 10^{22} cm^{-2}, and EM_1 and EM_2 are in units of 10^{56} cm^{-3}.

then become radiative (De Becker et al. 2006; Pollock 2012; Corcoran et al. 2011). However, there are a few wide binary systems that do not follow the $1/D$ variation, e.g., WR 11 (Rauw et al. 2000) and WR 22 (Gosset et al. 2009). The present X-ray light curves of WR 25 strongly support the idea that during the rise in X-ray emission around periastron passage the X-ray emission is primarily due to colliding winds (Willis et al. 1995; Stevens & Pittard 1999).

Using V of ∼8.03 mag, a distance of ∼3.24 kpc, a bolometric correction of −4.5 (Hamann et al. 2006), and an anomalous reddening of 4.5 mag (Hamann et al. 2006), the bolometric luminosity of WR 25 is calculated to be 1.25×10^{40} erg s^{-1}. The maximum and minimum values of $L_X/L_{\rm bol}$ for WR 25 are thus calculated to be $10^{-5.81}$ and $10^{-6.18}$, respectively. The derived value of $L_X/L_{\rm bol}$ during periastron passage is similar to that derived by Seward & Chlebowski (1982) using Einstein observations. During the phases of ∼0.03 and ∼0.7, the possible primary and secondary eclipse positions, where the WN and O-type stars contributed more in soft X-rays, respectively, the $L_X/L_{\rm bol}$ are calculated to be $10^{-6.5}$ and $10^{-6.31}$, respectively. These values of $L_X/L_{\rm bol}$ are similar to those obtained for other single WR and O-type stars (Skinner et al. 2010; Sana et al. 2006).

The hard X-rays from WR 25 appear to be a result of the collision of winds from binary companions. The gas in the colliding wind regions could either be adiabatic or radiative depending on the cooling parameter (χ_c) as $\chi_c = v_\infty^4 d/\dot{M}$ (Stevens et al. 1992), where v_∞ is in units of 10^3 km s^{-1}, d is the distance from the contact to star in units of 10^7 km, and $\dot{M}$ is in units of $10^{-7}\,M_\odot$ yr^{-1}. For $\chi_c \gtrsim 1$, the wind can be assumed to be adiabatic while, for $\chi_c \ll 1$, it is roughly isothermal. The cooling parameter is directly proportional to the distance of contact (d); as a consequence of this, $\chi_c \propto P_{\rm orb}^{2/3}$ (Stevens et al. 1992). This means that the shocked region will be adiabatic for longer period binaries. WR 25 is one of the longer orbital period binaries, indicating that the shocked region is adiabatic. Furthermore, if we assume that the contact of winds is close to the O-type star of WR 25, the value of χ_c is calculated to be >1, indicating an adiabatic wind in the shocked region. In our analysis, the abundances of O, Ne, Mg, Si, S, Ca, Ar, Fe, and Ni were found to be non-solar, which is expected from WR stars because they are in advanced evolutionary stages. The non-solar abundances of these elements could be due to the presence of hot plasma near the surface of the O4 star, due to the collision of strong supersonic winds from the WN6 star with the less powerful supersonic wind from the O4 star. For wide binaries, Pittard & Stevens (2002) showed that WR winds dominate the X-ray luminosity. Luo et al. (1990) and Myasnikov & Zhekov (1993) have also found that the shocked WR stellar wind dominates the X-ray emission for WR+O systems in the adiabatic limit. Furthermore, the shocked volume and the emission measured near the O-type star may be dominated by WN winds; therefore, the X-ray emitting plasma also shows non-solar abundances. When we compared the derived values of abundances of different elements for WR 25 with other WN-type stars, we found that the abundances of Ne and S in WR

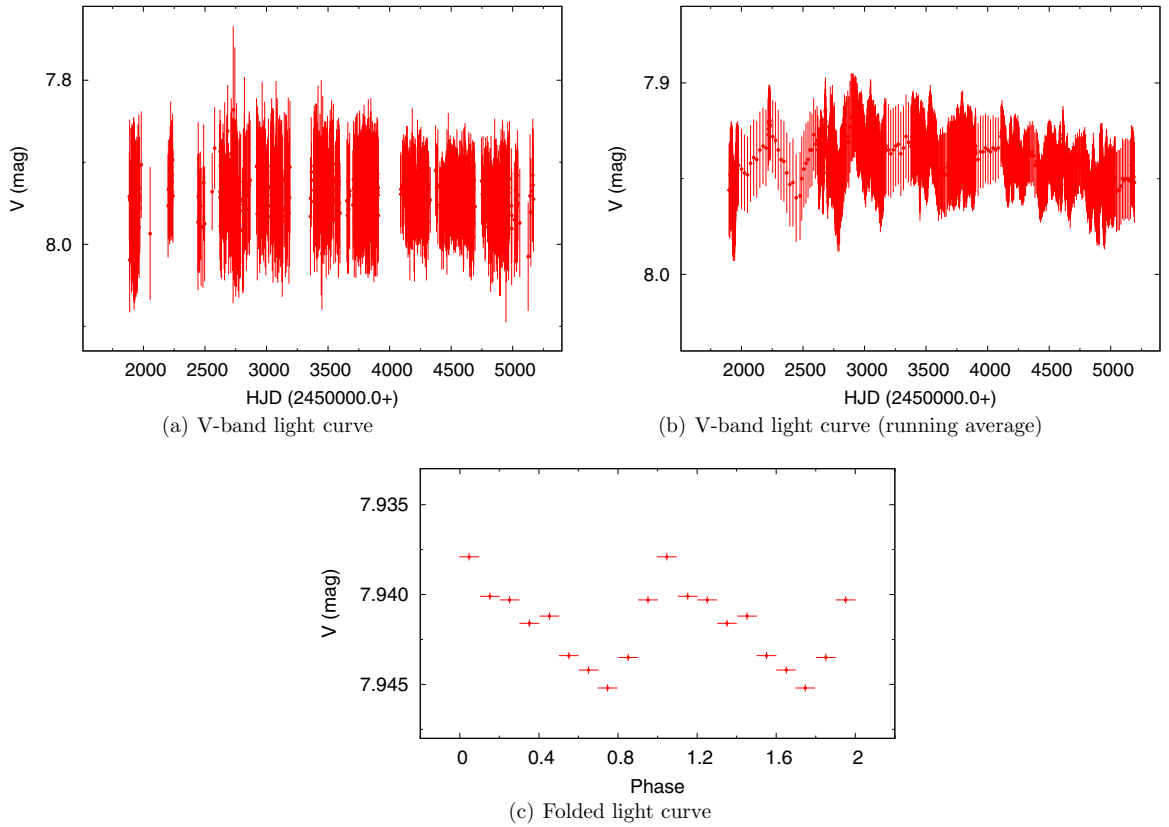

(a) V-band light curve (b) V-band light curve (running average)

(c) Folded light curve

Figure 6. (a) *V*-band light curve WR 25 as observed in ASAS, (b) light curve after smoothing (see the text for details), and (c) folded light curve of WR 25 using the ephemeris HJD = 2,451,598.0 + 207.85E as derived by Gamen et al. (2006).

(A color version of this figure is available in the online journal.)

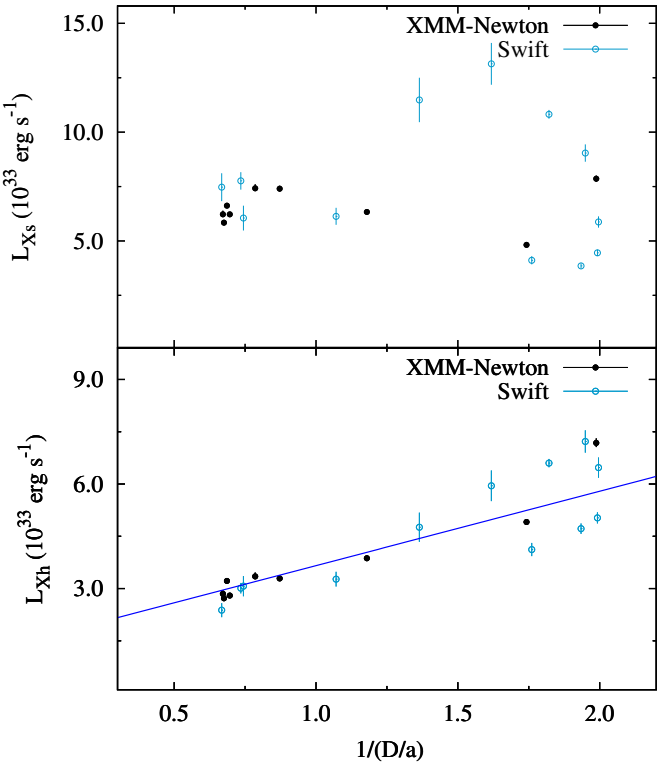

Figure 7. X-ray luminosity as a function of inverse of binary separation in soft and hard X-ray bands.

(A color version of this figure is available in the online journal.)

25 are similar to that of WN-type stars (Smith & Houck 2005; Ignace et al. 2007)

The light curve of WR 25 in the *V* band shows minimum light near phase 0.75, which could be a possible position of eclipse when the WN star is behind the O star. It appears that the WN star is brighter than the O-type star in the WR 25 system; therefore, we may observe an eclipse near phase 0.75. Hamann et al. (2006) also showed that O-type stars contribute a minimum of 15% to the total light of the system in the *V* band and Gosset et al. (1994) noticed the photometric variation in WR 25 with a variability amplitude of 0.02 mag in the Strömgren *b* band on a time scale of ∼250 days. Many other WR binaries also show phase-locked variability in the optical band and the variability is attributed to their binary nature (Lamontagne et al. 1996). The presence of eclipses in X-ray and optical light curves indicates that the orbital plane of WR 25 has a high inclination angle. The minimum of the *V*-band light curve is consistent with the phase minimum at ∼0.7 of the soft X-ray light curve. However, unlike to the soft X-ray light curve, we could not see any other minimum in the *V*-band light curve near phase 0.03, where $N_{\rm H}^{\rm local}$ was also found to be maximum. This could be due to the poor phase coverage of the *V*-band light curve.

The analysis of the present data shows that WR 25 is a colliding wind binary with an orbital period of ∼208 days, where the hard X-rays could be due to the collision zone while soft X-rays could be attributed to individual components.

We thank the referee for his/her comments and suggestions that helped to considerably improve the manuscript. This work uses data obtained by *XMM-Newton*, an ESA science mission

with instruments and contributions directly funded by ESA Member States and the USA (NASA). We acknowledge the *Swift* data archive and the UK *Swift* Science Data Center.

Facilities: XMM, *Swift*

REFERENCES

Abbott, D. C., & Conti, P. S. 1987, ARA&A, 25, 113
Antokhin, I. I., Rauw, G., Vreux, J.-M., & van der Hucht, K. A. 2003, in ASP Conf. Proc. 305, Magnetic Fields in O, B and A Stars: Origin and Connection to Pulsation, Rotation and Mass Loss, ed. L. A. Balona, H. F. Henrichs, & R. Medupe (San Francisco, CA: ASP), 383
Arnaud, K. A. 1996, in ASP Conf. Ser. 101, Astronomical Data Analysis Software and Systems V, ed. G. H. Jacoby & J. Barnes (San Francisco, CA: ASP), 17
Berghoefer, T. W., Schmitt, J. H. M. M., Danner, R., & Cassinelli, J. P. 1997, A&A, 322, 167
Bhatt, H., Pandey, J. C., Kumar, B., Sagar, R., & Singh, K. P. 2010a, NewA, 15, 755
Bhatt, H., Pandey, J. C., Kumar, B., Singh, K. P., & Sagar, R. 2010b, MNRAS, 402, 1767
Burrows, D. N., Hill, J. E., Nousek, J. A., et al. 2005, SSRv, 120, 165
Cherepashchuk, A. M. 1976, PAZh, 2, 356
Corcoran, M. F., Pollock, A. M. T., Hamaguchi, K., & Russell, C. 2011, arXiv:1101.1422
Crowther, P. A. 2007, ARA&A, 45, 177
Crowther, P. A., & Dessart, L. 1998, MNRAS, 296, 622
Crowther, P. A., Hillier, D. J., & Smith, L. J. 1995, A&A, 293, 403
De Becker, M., Rauw, G., Pittard, J. M., et al. 2004, A&A, 416, 221
De Becker, M., Rauw, G., Sana, H., et al. 2006, MNRAS, 371, 1280
Doom, C. 1987, RPPh, 50, 1491
Feldmeier, A., Puls, J., & Pauldrach, A. W. A. 1997, A&A, 322, 878
Gamen, R., Gosset, E., Morrell, N., et al. 2006, A&A, 460, 777
Gorenstein, P. 1975, ApJ, 198, 95
Gosset, E., Nazé, Y., Claeskens, J.-F., et al. 2005, A&A, 429, 685
Gosset, E., Nazé, Y., Sana, H., Rauw, G., & Vreux, J.-M. 2009, A&A, 508, 805
Gosset, E., Rauw, G., Manfroid, J., Vreux, J.-M., & Sterken, C. 1994, in NATO ASIC Proc. 436, The Impact of Long-Term Monitoring on Variable Star Research: Astrophysics, ed. C. Sterken & M. De Groot (Dordrecht: Kluwer), 101
Gräfener, G., & Hamann, W.-R. 2005, A&A, 432, 633
Hamann, W.-R., Gräfener, G., & Liermann, A. 2006, A&A, 457, 1015
Ignace, R., Cassinelli, J. P., Tracy, G., Churchwell, E., & Lamers, H. J. G. L. M. 2007, ApJ, 669, 600
Ignace, R., Oskinova, L. M., & Brown, J. C. 2003, A&A, 408, 353
Jansen, F., Lumb, D., Altieri, B., et al. 2001, A&A, 365, L1
Lamontagne, R., Moffat, A. F. J., Drissen, L., Robert, C., & Matthews, J. M. 1996, AJ, 112, 2227
Lomb, N. R. 1976, Ap&SS, 39, 447
Lucy, L. B. 1982, ApJ, 255, 286
Lucy, L. B., & White, R. L. 1980, ApJ, 241, 300
Luo, D., McCray, R., & Mac Low, M.-M. 1990, ApJ, 362, 267
Meynet, G., & Maeder, A. 2005, A&A, 429, 581
Morrison, R., & McCammon, D. 1983, ApJ, 270, 119
Myasnikov, A. V., & Zhekov, S. A. 1993, MNRAS, 260, 221
Nazé, Y. 2009, A&A, 506, 1055
Nazé, Y., Mahy, L., Damerdji, Y., et al. 2012, A&A, 546, A37
Niedzielski, A., & Skorzynski, W. 2002, AcA, 52, 81
Oskinova, L. M. 2005, MNRAS, 361, 679
Owocki, S. P., Castor, J. I., & Rybicki, G. B. 1988, ApJ, 335, 914
Pittard, J. M., & Stevens, I. R. 2002, A&A, 388, L20
Plucinsky, P. P., Beardmore, A. P., DePasquale, J. M., et al. 2012, Proc. SPIE, 8443, 12
Pojmanski, G. 2002, AcA, 52, 397
Pollock, A. M. T. 1987, ApJ, 320, 283
Pollock, A. M. T. 2012, in ASP Conf. Ser. 465, Proceedings of a Scientific Meeting in Honor of Anthony F. J. Moffat, ed. L. Drissen et al. (San Francisco, CA: ASP), 308
Pollock, A. M. T., & Corcoran, M. F. 2006, A&A, 445, 1093
Prilutskii, O. F., & Usov, V. V. 1976, SvA, 20, 2
Raassen, A. J. J., van der Hucht, K. A., Mewe, R., et al. 2003, A&A, 402, 653
Rauw, G., Stevens, I. R., Pittard, J. M., & Corcoran, M. F. 2000, MNRAS, 316, 129
Rauw, G., Vreux, J.-M., Stevens, I. R., et al. 2002, A&A, 388, 552
Sana, H., Rauw, G., Nazé, Y., Gosset, E., & Vreux, J.-M. 2006, MNRAS, 372, 661
Sana, H., Stevens, I. R., Gosset, E., Rauw, G., & Vreux, J.-M. 2004, MNRAS, 350, 809
Scargle, J. D. 1982, ApJ, 263, 835
Seward, F. D., & Chlebowski, T. 1982, ApJ, 256, 530
Skinner, S. L., Zhekov, S. A., Güdel, M., & Schmutz, W. 2002a, ApJ, 579, 764
Skinner, S. L., Zhekov, S. A., Güdel, M., & Schmutz, W. 2002b, ApJ, 572, 477
Skinner, S. L., Zhekov, S. A., Güdel, M., & Schmutz, W. 2007, MNRAS, 378, 1491
Skinner, S. L., Zhekov, S. A., Güdel, M., Schmutz, W., & Sokal, K. R. 2010, AJ, 139, 825
Smartt, S. J. 2009, ARA&A, 47, 63
Smartt, S. J., Eldridge, J. J., Crockett, R. M., & Maund, J. R. 2009, MNRAS, 395, 1409
Smith, J.-D. T., & Houck, J. R. 2005, ApJ, 622, 1044
Smith, R. K., Brickhouse, N. S., Liedahl, D. A., & Raymond, J. C. 2001, ApJ, 556, 91
Stevens, I. R., Blondin, J. M., & Pollock, A. M. T. 1992, ApJ, 386, 265
Stevens, I. R., & Pittard, J. M. 1999, in IAU Symp. 193, Wolf–Rayet Phenomena in Massive Stars and Starburst Galaxies, ed. K. A. van der Hucht, G. Koenigsberger, & P. R. J. Eenens (San Francisco, CA: ASP), 289
Strüder, L., Aschenbach, B., Bräuninger, H., et al. 2001, A&A, 375, L5
Turner, M. J. L., Abbey, A., Arnaud, M., et al. 2001, A&A, 365, L27
Usov, V. V. 1992, ApJ, 389, 635
van der Hucht, K. A. 1992, A&ARv, 4, 123
van der Hucht, K. A. 2001, NewAR, 45, 135
Willis, A. J., Schild, H., & Stevens, I. R. 1995, A&A, 298, 549
Zhekov, S. A. 2012, MNRAS, 422, 1332